CHAPTER 66

SAND CONCENTRATION IN AN OSCILLATORY FLOW

by W.T. Bakker[1]

0. Abstract.

     In this paper first a numerical model is described con-
cerning the velocity distribution in an oscillatory flow, res-
pectively without and with resultant current. From the mo-
mentaneous velocity gradients eddy viscosities are derived.
Using the approach of VANONI [1], a numerical model is given
for the calculation of sediment concentration and suspended
sediment transport. In order to give reliable results, the
bed-load concentration should be known. This will be investi-
gated in the future; at the moment the model only provides
qualitative results.

1. Introduction.

     This paper deals about the calculation of suspended
sediment transport in an oscillatory flow, with or without
resultant current. The approach is the same as the one of
VANONI [1], however unstationary effects have been taken into
account: the sediment transport is found by multiplying mo-
mentaneous concentrations with momentaneous velocities and
integrating these over the wave period.
The investigation only covers a part of a larger schedule for
research:
a. Computation of the velocity distribution in a horizontally
   oscillating flow, as occurs for instance in a oscillatory
   water tunnel. Assumptions and computations are given in ch.
   2.
b. From the velocity distributions the gradient of the velo-
   cities and the eddy viscosity is derived, after which the
   suspended load can be calculated. The method is treated in
   ch. 4.
c. For the solution given ad b, a boundary condition near the
   bottom is needed and therefore investigations have to be
   made about the bottom transport. These investigations still
   have to be carried out. As the sand concentration at the
   bottom determines the concentration in the higher layers,
   this means, that the present investigation only can give
   qualitative results.
d. The results of the mentioned computations should be checked
   in a oscillatory wave tunnel. Also this check still has to
   be made.

---

[1] Senior Scientific Officer, Techn. Univ. of Delft,
Head of Study Dept. Vlissingen, Rijkswaterstaat.

e. The following step is the adding of a constant additional
current. Ch. 3 deals with the computation.

f, g. Again the same procedure can be applied, including the cal-
culation of the sediment transport (f, chapter 4) and the
check in an oscillatory water tunnel (g).

h,i,j. Finally the three-dimensional problem has to be tackled:
waves and currents making an angle with each other. The
way of solving is in principle the same (h: investigation
water motion, i: investigation sediment motion), however
now checks in prototype and hydraulic model should be made
(j). The three-dimensional problem will not be treated
here: the paper ends with a conclusion (chapter 5).

2. Numerical computation of the velocity distribution in an os-
cillatory flow.

2.1. Assumptions.

2.1.1 Apart from turbulent fluctuations, the flow is assumed to
be horizontally directed and to be uniform in horizontal
direction. Hence, the velocity u is assumed to be only a
function of the vertical coordinate z and of the time t,
but no function of the horizontal coordinate x. The pres-
sure gradient is acting in horizontal direction; the
pressure is only a function of x and t.

2.1.2 In the inner part of the fluid, a turbulent shear stress
is assumed, according to the assumptions of PRANDTL [2]
equal to:

$$\tau = \rho l^2 \frac{\partial u}{\partial z} \left| \frac{\partial u}{\partial z} \right| \qquad (1)$$
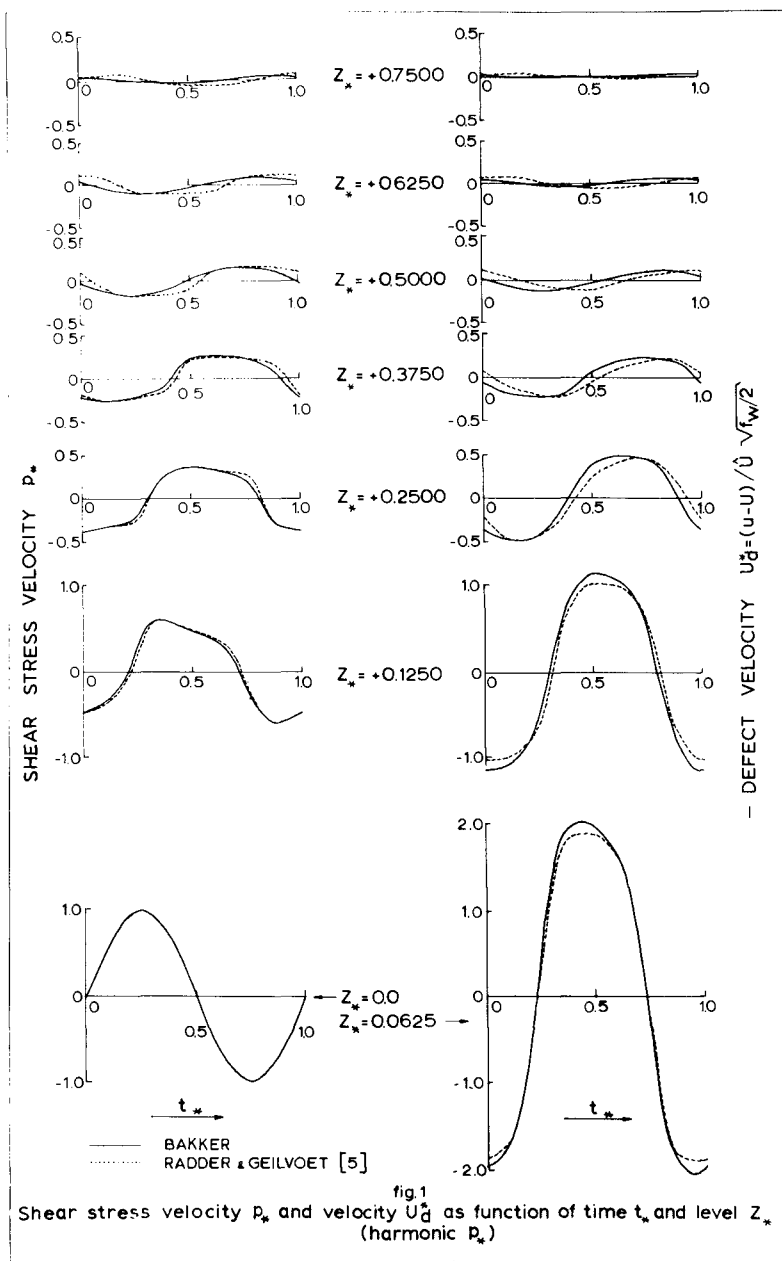
in which τ is the shear stress, taken positive when ac-
ting in positive x-direction from the upper layer to the
lower layer. ρ is the specific density of the fluid, l is
the mixing length, being according to von KARMAN [3] pro-
portional to the distance z from the theoretical bottom:

$$l = xz \qquad (2)$$

x being the von KARMAN constant.

2.1.3 With respect to the boundary conditions, two cases $\underline{a}$ and $\underline{b}$
are considered:

$\underline{a}$ The fluid motion far from the bottom is such, that a har-
monic shear stress velocity at the bottom results;

$\underline{b}$ The velocity U of the fluid far from the bottom elapses
harmonically in course of time.

The bottom is assumed to be hydraulically rough. The velo-
city at a distance z_0 above the theoretical bottom level is
assumed to be zero, z_0 is assumed to be .03 times the
ripple height.

2.2. Derivation of the equation for the shear stress velocity.
The acceleration on a rectangular element of the fluid
is caused by the gradient of the shear stress in vertical

fig.1
Shear stress velocity p_* and velocity U_d^* as function of time t_* and level Z_*
(harmonic p_*)

direction z and the gradient of the normal pressure p_r in horizontal direction x:

$$\rho \frac{\partial u}{\partial t} = \frac{\partial \tau}{\partial z} - \frac{\partial p_r}{\partial x} \tag{3}$$

Far from the bottom, the shear stress is reduced to zero, as well as $\frac{\partial \tau}{\partial z}$. There, according to (3), $\frac{\partial u}{\partial t}$ will be no function of z, as p_r is assumed to be no function of z.
The velocity far from the bottom, of which the variable part is only a function of t (not of z) will be called U, being determined by:

$$\rho \frac{\partial U}{\partial t} = -\frac{\partial p_r}{\partial x} \tag{4}$$

We assume U only a function of t in this section.
JONSSON [4] calls u-U the "defect velocity" defined by:

$$u_d = u - U \tag{5}$$

The defect velocity has a physical meaning: it is the velocity which occurs when considering the case of an oscillating plate in a fluid being at rest at infinity instead of the case of a moving fluid above a stable bottom. Subtracting (4) from (3) and substitution of u_d from (5) gives:

$$\frac{\partial u_d}{\partial t} = \frac{\partial (\tau/\rho)}{\partial z} \tag{6}$$

or, introducing (1) and (2):

$$\frac{\partial u_d}{\partial t} = \frac{\partial (xz \frac{\partial u}{\partial z} |xz \frac{\partial u}{\partial z}|)}{\partial z} \tag{7}$$

This equation can be transformed into an equation for the internal shear stress velocity. In this paper this will be denoted by p instead of U_*, as the star as index will be reserved for dimensionless quantaties. Define p as:

$$p = sign(\tau) . \sqrt{\tau/\rho} \tag{8}$$
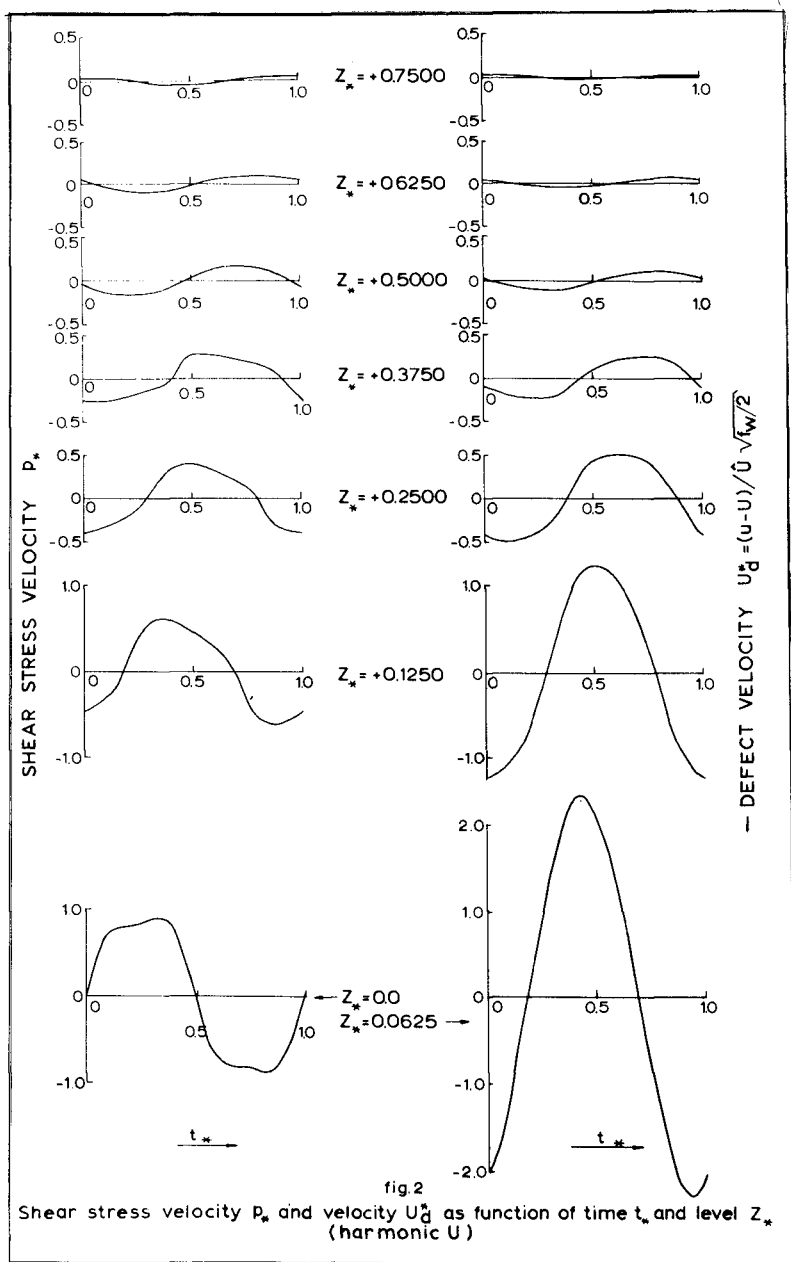
From (1) and (2):

$$p = xz \frac{\partial u}{\partial z} \tag{9}$$

According to (5), U in (9) may be replaced by u_d, and hence, differentiation of eq (7), to z and multiplying by xz gives a differential equation for the internal shear stress velocity:

$$\frac{\partial p}{\partial t} = xz \frac{\partial^2 (p|p|)}{\partial z^2} \tag{10}$$

This equation can be solved by numerical procedures, as will be shown in the appendix. For this goal, first the equation has been made dimensionless by introducing the dimensionless variables:

fig.2
Shear stress velocity p_* and velocity U_d^* as function of time t_* and level Z_*
(harmonic U)

$p_* = p/\hat{p}_b$ where $\hat{p}_b$ = the maximum shear stress, exerted
                                    at the bottom

$t_* = t/T$ where T = the period of the periodical
                                    motion

$z_* = z/Z$ where $Z = x\hat{p}_b T$ = a reference length

Then eq (10) reduces to:

$$\frac{\partial p_*}{\partial t_*} = z_* \frac{\partial^2 (p_* |p_*|)}{\partial z_*^2} \tag{11}$$

The equation has first been solved with the assumption of a
sinusoidal shear stress velocity p^*_b at the bottom, i.e. with
the following boundary conditions:

$$p^*_b = \text{SIN } 2 \pi t_* \quad \text{for} \quad z_* = 0 \tag{12}$$

and $p^* \equiv 0$ for $z_* = z^*_{max}$ \hfill (13)

The upper boundary should be $p_* = 0$ for z_* is infinite; how-
ever as this values is difficult to obtain numerically, it
has been replaced by z^*_{max}. From an approximate analytical
solution it was found that the maximum value of p_* at $z_* = 1$
was about $3^o/oo$ of the maximum value at the bottom; there-
fore for most computations $z^*_{max} = 1$ has been chosen. Also
numerical computations with larger z^*_{max} always gave low
values of p_* at $z_* = 1$.

2.3. The initial condition.
        As initial condition has been chosen:

$$p_* \equiv 0 \quad \text{for } t_* = 0 \tag{14}$$

Considering the symmetry of the motion, it is reasonable
to assume, that for the final solution at every level and
time is valid:

$$p_* (t_*) = -p_* (t_* + \tfrac{1}{2}) \tag{15}$$

As the initial condition does not coincide with the perio-
dical solution of p_* at any time, the initial condition
gives an initial disturbance, which fades away after a num-
ber of periods calculation. In order to fasten the process
of convergence to the periodic solution, corrections were
applied after each of the first calculated wave periods
(up to half of the total number of calculated periods). If
the calculated velocity after $(n+\tfrac{1}{2})$ T was a and after nT
was b, a correction (b-a)/2 was applied. This way of correc-
ting attenuated the initial effect very soon and after the
first half number of periods the motion remained very well
periodic during the computation.

2.4. Calculation of p and U.
        In the appendix an explicite method of numerical com-
putation is described for solving eq (11). The solution
has been checked by RADDER and GEILVOET, using an implicite
method [5]. The implicite and the explicite method showed
to be about equivalent, although illconditioned matrices

could make the implicite results less reliable when p_b was
about zero[5]. In fig. 1 (left-hand side) the results of the
explicite and implicite method are shown: for various levels
z_* curves are drawn indicating p_* as function of t_*. In fig.
5^a, left-hand side, curves are drawn showing p_* as function
of z_* for various values of t_*.

By numerical integration the dimensionless defect velo-
city $u_d^* = u_d/\hat{p}_b$ can be found. Using (9):

$$u_d^* = \frac{1}{x} \int_{z_*}^{\infty} \frac{p_*}{z_*} \, dz_* \tag{16}$$

For the lower boundary of integration z_* the various levels
on which p_* has been computed can be substituted. The right
hand side of fig. 1 shows u_d^* as function of t_*, at various
levels z_*, fig. 5^b gives u_d^* as function of z_* for various
values of t_*.

At a distance $z=z_o$, u equals zero, according assumption
2.1.3, and thus u_d^* equals $-U$, according to (5). By assuming
the values of z_* at the successive levels for which p_* has
been computed, equal to $0.03 \; r^*=0.03 \; r/Z$, for the correspon-
ding values of the dimensionless ripple height r_* the dimen-
sionless velocity $U_*=U/\hat{p}_b$ far from the bottom can be found.
Then according to (5), $U_*=U/\hat{p}_b$ equals $u_d^* + U_*$. Fig. 5 shows
velocity profiles u_* for various t_*.

From the value of U_* a first-order approximation of the
friction coefficient can be derived.

A usual definition of the friction coefficient is (vide
for instance JONSSON [6], [7]:

$$f_w = \frac{\hat{\tau}}{\frac{1}{2}\rho \hat{U}_h^2} \tag{17}$$

where τ denotes the top shear stress, caused by a harmonic
velocity with amplitude U_h far from the bottom. Of course,
then τ is not harmonic in course of time.

As in the calculated case U does not elapse harmoni-
cally, it does not seem correct to replace (17) by:

$$f_w \overset{?}{=} \frac{2 \hat{p}_b^2}{\hat{U}_*^2}$$

Instead, the first and third harmonic U_1 and U_3 of U
have been calculated and for f_w the relationship has been
assumed:

$$f_w = \frac{3\pi}{8} \frac{2\hat{p}_b^2}{U_*^2} \tag{18}$$

The coefficient "$3\pi/8$" originates from the consideration,
that a schematized harmonic shear stress should have an
amplitude, equal to $8/3\pi$ times the top value of the real,
non-harmonic one in order to be equivalent with respect to the
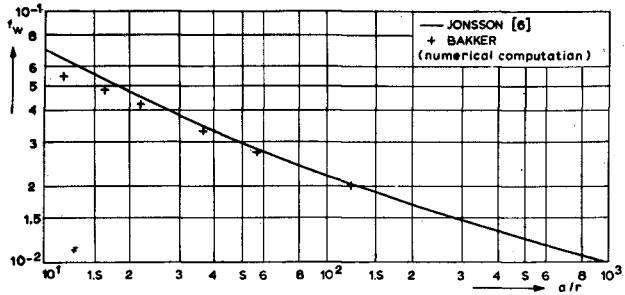
fig. 3 FRICTION COEFFICIENT f_w VERSUS RATIO STROKE LENGTH/RIPPLE HEIGHT
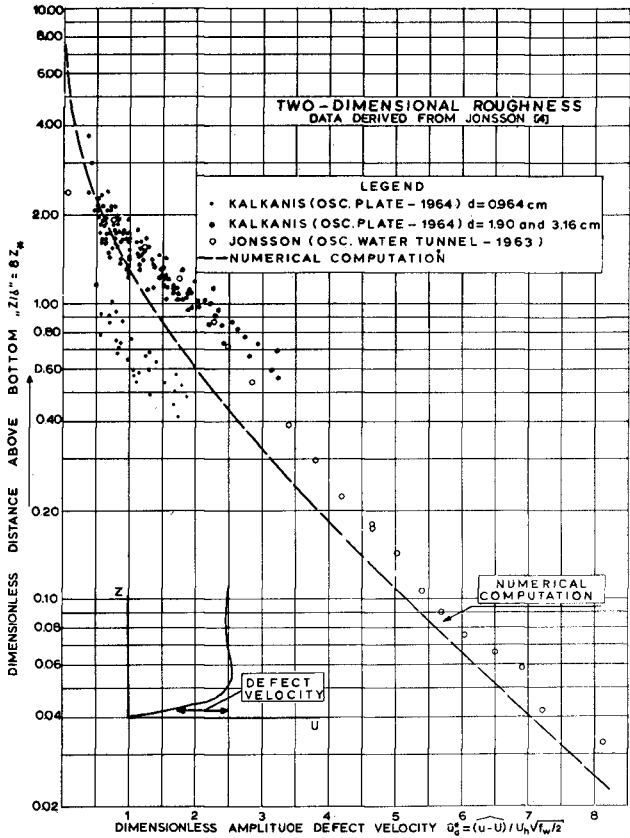
fig. 4 ENVELOPE OF DEFECT VELOCITY DISTRIBUTIONS
COMPARISON NUMERICAL RESULTS WITH DATA

energy dissipation [8], [9].

It will be reminded that in (18) $U_1/\hat{p}_b$ equals U_1*. Thus, starting from a certain level on which p_* and U_* have been computed and assuming this level z_0* equal to $0.03r_*$, one finds f_w for $r_*=z_0*/0.03$ from (18). On the other hand, z_0* can be expressed in the ratio stroke length /ripple height a/r:

$$z_0* = 0.03 r_* = 0.03\,\frac{r}{z} = 0.03\,\frac{r}{x\hat{p}_b\,T} = \frac{0.03}{2\pi x\,\sqrt{f_w/2}} \cdot \frac{r}{UT/2\pi}$$

$$\frac{r}{a} = \frac{2\pi x\,\sqrt{f_w/2}}{0.03} \cdot z_0* \tag{19}$$

in which f_w is known from (18).

As z_0* can be, in principle every level for which u_* has been calculated, from one numerical computation (with a small Δz_*) a number of combinations of a/r and f_w can be found. These are given in fig. 3.

However, still the assumed coefficient $3\,\pi/8$ as well as the stated boundary condition (U in this way, that a harmonical shear stress velocity results) seems artificial and not quite logical. In a more elegant way, one can add a third harmonic to p_* ($\hat{p}_b$ then being defined as the amplitude of the first harmonic of p_b) and minimize by an iteration procedure the third harmonic of U_*, starting from u_d* at a certain level z_0*. Then f_w can be found as:

$$f_w = 2\,\frac{\hat{p}_b*^2}{\hat{U}_*^2} \tag{20}$$

where $\hat{p}_b*$ equals the top value of the combination of the first and third harmonic[1].

In fig. 2, analogous to fig. 1, a third harmonic equal to 17% of the first one and having a phase difference of 15° with the first one, has been added to the shear stress velocity.[2]
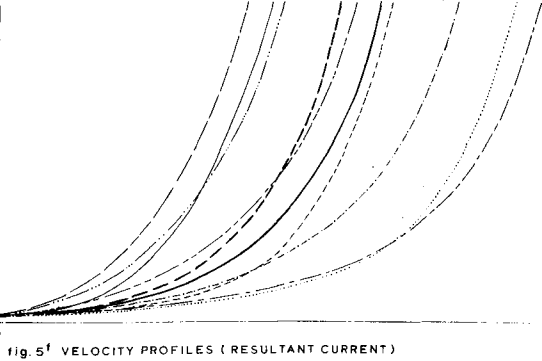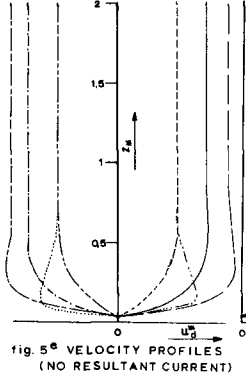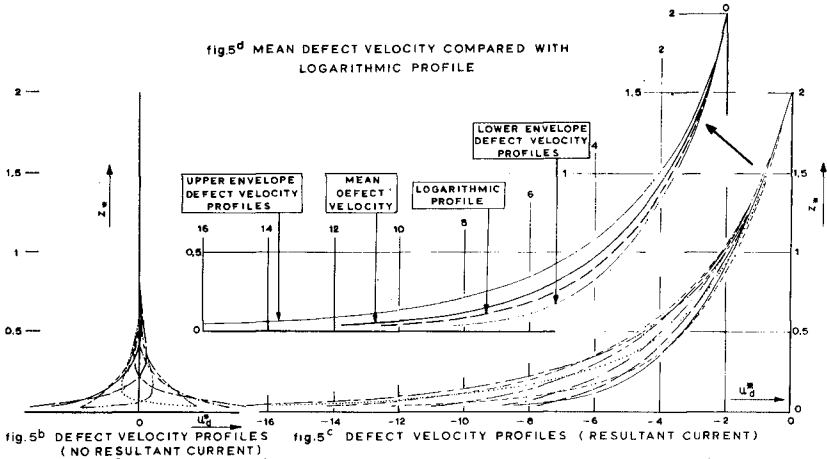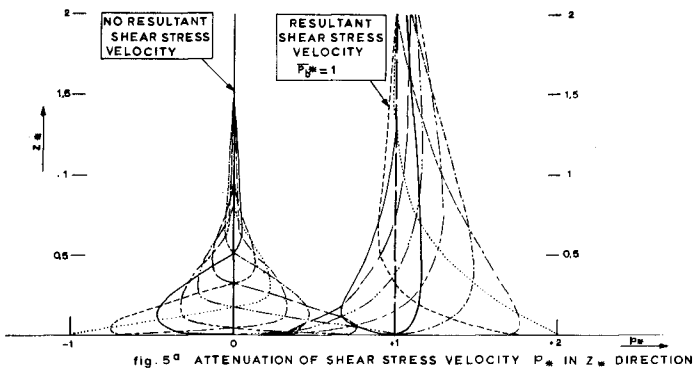
By this, the third harmonic of U_* at a level $z_*=0.0625$ dropped to 1% of the first one (being originally 15%).

As in this particular case, the value of $\hat{p}_b$ appeared to be 10% smaller than $\hat{p}_b$, eq (20) gave considerable lower friction coefficients than (18). This is a reason for future researsch; now only the way of solution has been indicated.

As Z equals $x\hat{p}_b T$, i.e. $2\pi x\,a\sqrt{f_w/2}$, and f_w can be found from a/r, the dimensionless numerical model can be connected with the prototype.

---

[1] for reasons of symmetry of the second harmonic of as well p_b* as U_* should be zero.

[2] i.e. $p_b = \sin \omega t + 0.17 \sin(3\omega t + 15^{\circ})$

fig. 5ᵃ ATTENUATION OF SHEAR STRESS VELOCITY P∗ IN Z∗ DIRECTION

fig.5ᵈ MEAN DEFECT VELOCITY COMPARED WITH
LOGARITHMIC PROFILE

fig.5ᵇ DEFECT VELOCITY PROFILES   fig.5ᶜ DEFECT VELOCITY PROFILES (RESULTANT CURRENT)
(NO RESULTANT CURRENT)

fig. 5ᵉ VELOCITY PROFILES   fig. 5ᶠ VELOCITY PROFILES (RESULTANT CURRENT)
(NO RESULTANT CURRENT)

2.5. Comparison with measurements and other theories.
        Fig. 3 shows a comparison between the friction coeffi-
cient found by JONSSON [6] and the results of the numerical
computation. Fig. 4 shows a graph in which the data is plot-
ted collected by JONSSON [4] from his experiments described
in [6] and from experiments of KALKANIS [11].[1]) Furthermore,
the amplitude of the dimensionless defect velocity u_d^* found
from the computer program is plotted versus the dimension-
less height above the bottom z_*.
The correspondence is quite satisfactory.
        In fig. 3 the obtained friction coefficients are com-
pared with the results of JONSSON [6] . For low values of
a/r the numerical model gives somewhat lower results.

3.   Oscillatory flow plus resultant current.

        A shear stress velocity, constant over the vertical and
in the time, results according to (16) into a logarithmic
velocity profile, being a good approximation of the velocity
profile of a stationary current. Therefore, the approximation
p=constant (say $\bar{p}_b$) was assumed to be good enough to repro-
duce the velocity profile in the layers of the fluid above
the turbulent boundary layer. In this section U (defined by
(4)) will be assumed to consist of a logarithmic part,
being zero at $z=z_{max}$ and an unstationary part U' being no
function of z. U' thus denotes the velocity at $z=z_{max}$:

$$U = \frac{\bar{p}_b}{x} \ln \frac{z}{z_{max}} + U'(t)$$

z_{max} is assumed to be so large, that $\frac{\partial \tau}{\partial z}$ in eq (3) can be
neglected. As in sect. 2.2 the defect velocity u_d will be
defined as the deviation of u from U, occuring in the tur-
bulent boundary layer, cf eq (5).
        The combination of an oscillatory flow plus a resul-
tant current has been simultated with the explicite com-
puter program by adding, after some wave periods of a normal
run, a constant shear stress velocity over the whole stretch
from bottom to z^*_{max}. After that, the calculation was con-
tinued over a number of wave periods until a periodical
shear stress velocity resulted. The curves of p_* as function
of z_* for various t_* are plotted in fig. 5[a], together with
the analogous ones in the case that no resultant shear
stress is present. It shows, that the variation of the shear
stress velocity attenuates much more slowly in upward direc-
tion in the case with a resultant shear stress velocity than
in the case without and further more, that the envelope of
minimum shear stress velocity at each level tends faster to
the imposed constant shear stress velocity than the envelope

----

[1]) "z/δ " in fig. 1[d] of [4] has been transferred to z_*.
      From [10] , eq (4.4), (4.14) and (4.18) it shows that
      $\delta = (0.04 \quad \pi a \quad \sqrt{f_w/2})/x$ and as $Z=2 \quad \pi x a \quad \sqrt{f_w/2}$, it
      appears that "z/δ "= 8 z_*, as x = 0.4.

of the maxima. Because of the last-mentioned feature, the mean
shear stress velocity inside the fluid differs from the mean
shear stress velocity, imposed in the beginning.

In fig. 5^a with a thick drawn line the mean shear stress
velocity has been indicated, with an interrupted line the im-
posed one.

Fig. 5^c shows the integration from p_* to U_d^* carried out
in the same way as done for oscillatory flow without current
in fig. 5^b, i.e. by integrating, according to (16), taking as
upper boundary $z_* = z^*_{max}$ [1]).

In fig. 5^d, analogous to fig. 5^c, with a thick drawn line
the mean value of u_d^* has been indicated, with an interrupted
line the logarithmic profile, resulting from a stationary
shear stress velocity equal to $\bar{p}_b$.

From fig. 5^c figure 5^f can be derived, by a parallel
shift of the velocity distributions, in this way, that the ve-
locity at a distance $z_o^* = 0.03\ r_*$ equals zero. This gives the
real velocity distribution for various times t_*. Also the line
of the mean value of u_d^* and the line of the logarithmic pro-
file are shifted (thick drawn-, resp. interrupted line in fig.
5^f) and one observes, that the time-average of the velocity
above the bottom will be larger than one would find from the
logarithmic profile (interrupted line), which would result
when leaving the variation in the shear stress velocity out
of consideration. Far from the bottom the interrupted line
and the drawn line will be parallel. This means, that for a
given value of the average mean shear stress velocity the
mean velocity over the depth will be larger with an oscilla-
tory motion than without. If the mean shear stress velocity
$\bar{p}_b$ equals the amplitude of the variation $\hat{p}_b$ [2]) from the nu-
merical computation it appeared that this increase is of the
same order as this shear stress velocity.

Furthermore, comparing fig. 5^b with fig. 5^c, it shows
that the same variation of the shear stress velocity $\hat{p}_b^*$ re-
sults in a much larger variation of u_d^* when a resultant cur-
rent is present than when there is not. This is the effect
of the deeper intrusion into the fluid of the variation of
the shear stress when a resultant current is present (cf.
fig. 5^a). This results in a larger variation of U (compare
fig. 5^e with fig. 5^f) with the same amplitude $\hat{p}_b$.
Summarizing and concluding:
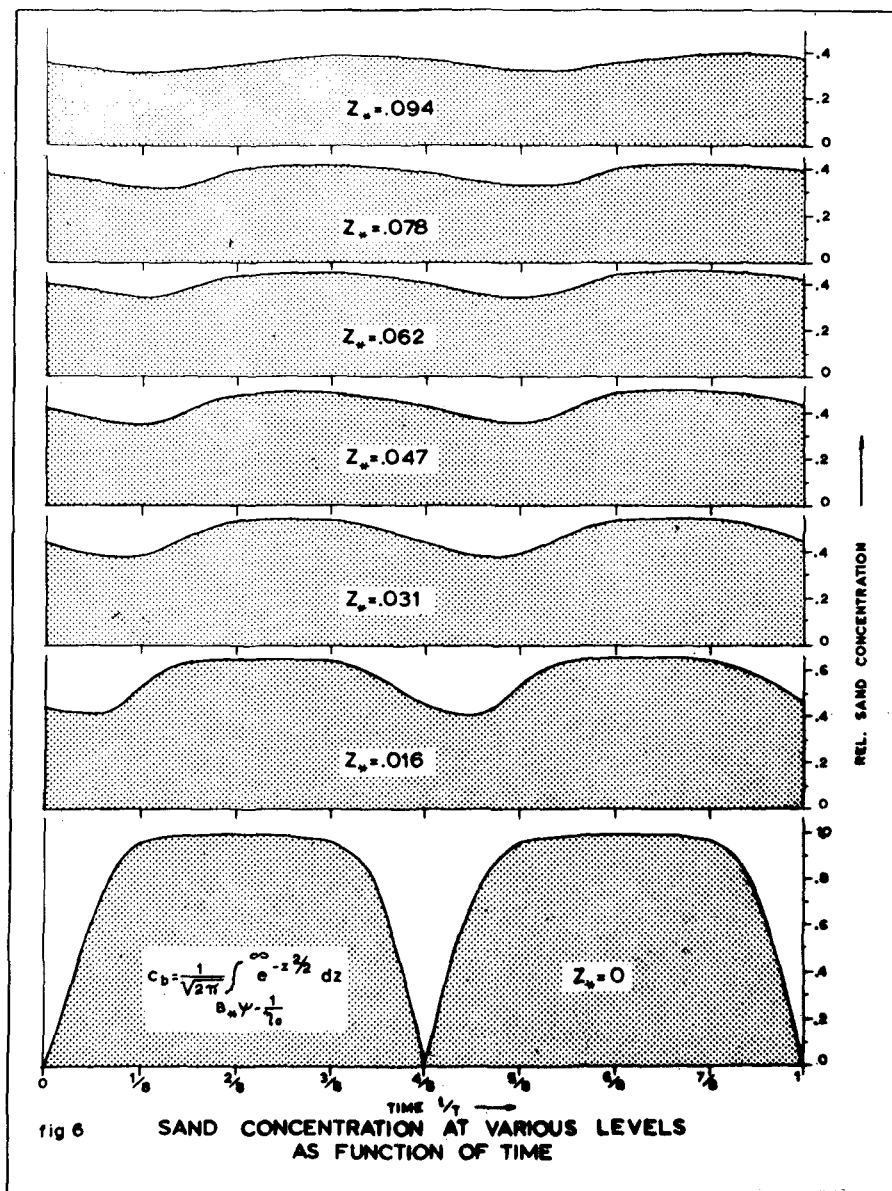
In a stationary current without oscillatory flow U is
proportional to the bottom shear stress p_b:

$$\bar{U} = \sqrt{\frac{2}{f_c}}\ p_b \ ;\ \text{where}\ \sqrt{\frac{2}{f_c}} = \frac{1}{h}\int_o^h \frac{1}{x}\ \ln\frac{z}{z_o}\ dz = \frac{C_h}{\sqrt{g}}$$

C_h being the Chezy coefficient and g the acceleration of gravi-
ty. Of an oscillatory flow is present one finds:

---

1) z^*_{max} has been chosen somewhat too small in fig. 5^c. This
   is no matter of principle.

2) Note, that the top value of p_b equals $\bar{p}_b + \hat{p}_b$.

fig 6   SAND CONCENTRATION AT VARIOUS LEVELS
              AS FUNCTION OF TIME

$$\bar{U} = \sqrt{\frac{2}{f_c}} \; \bar{p}_b + U_r$$

, where U_r is a positive residual velocity [1]) U_r is a function of $\hat{p}_b/\bar{p}_b$ and of a/r. Thus U_r can be hidden in a decreasing coefficient f_c.

and $\hat{U} = \hat{p}_b \sqrt{\frac{2}{f_w}}$ f_w decrease when apart from the oscillatory flow a current is present [2]).

The average value over the wave period of the bottom shear stress equals, when $\hat{p}_b \leqslant \bar{p}_b$:

$$\bar{\tau} = \overline{\left\{\bar{p}_b + \hat{p}_b \; \sin(\omega t + \varphi)\right\}^2} = \bar{p}_b^2 + \tfrac{1}{2} \hat{p}_b^2$$

$$\bar{\tau} = \tfrac{f_c}{2} (\bar{U} - U_r)^2 + \tfrac{f_w}{2} \hat{U}^2 \qquad\qquad (21)$$

Therefore, although the existance of U_r and the decrease of f_w, still an increase of the average shear stress can be expected by the presence of waves.

4. Sand concentration and sand transport.

    The calculation of the sand concentration is based on the equation:

$$\frac{\partial c}{\partial t} = \frac{\partial}{\partial z}(\varepsilon \frac{\partial c}{\partial z} + wc) \qquad\qquad (22)$$

Eq (22) is a continuity equation for the sediment. The right-hand part between the parentheses indicates the sediment flux in a vertical downward direction, w being the settling velocity, positive in negative z-direction, the first term indicating the turbulent exchange, the second one the settling. c is the sediment concentration. The turbulent exchange factor has been taken equal to the eddy viscosity ε, defined by:

$$\frac{\tau}{\rho} = \varepsilon \frac{\partial u}{\partial z} \qquad\qquad (23)$$

where, according to (1) and (2):

$$\varepsilon = x^2 z^2 \left|\frac{\partial u}{\partial z}\right| \qquad\qquad (24)$$

In a dimensionless shape, eq (22) reads:

$$\frac{\partial c}{\partial t_*} = \frac{\partial}{\partial z_*}(\varepsilon_* \frac{\partial c}{\partial z_*} + w_* c) \qquad\qquad (25)$$

where $\varepsilon_* = \varepsilon/x^2 \hat{p}_b^2 \; T \; (= \varepsilon T/Z^2)$ \qquad\qquad (26)

----

[1] from numerical computations it was found, that U_r is of the order of p_b, when $\hat{p}_b = \bar{p}_b$
[2] Reductions of 30% may occur when $p_b = \hat{p}_b$

DIMENSIONLESS VELOCITY U_*

VELOCITY
DISTRIBUTION
OSCILLATORY
FLOW PLUS
RESULTANT
CURRENT

DISTRIBUTION
OF SEDIMENT
TRANSPORT
$U * C$
(ROUGH BOTTOM)

DIMENSIONLESS SEDIMENT TRANSPORT $C . U_*$
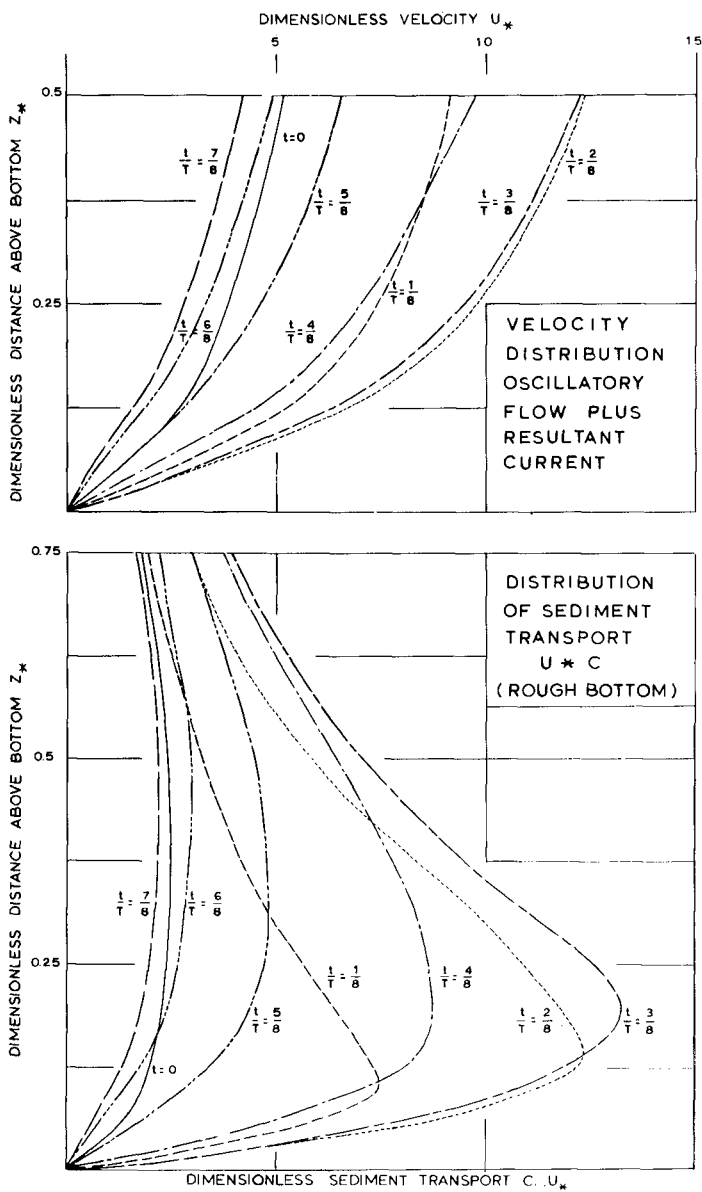
fig. 7 EXAMPLE OF VELOCITY DISTRIBUTION AND SEDIMENT TRANSPORT
IN AN OSCILLATORY FLOW WITH RESULTANT CURRENT.

or, from $(24): \varepsilon_* = Y_* |p_*|$ (27)

and $w = w/x \; \hat{p}_b \; (= w T/Z)$ (28)

w_*, indicating the ratio between the falling distance of a grain in still water in a wave period on one hand and the decay distance Z of the shear stress on the other hand, also can be compared with $"Z"="w/x \; V_*"$ as defined by EINSTEIN[12], where V_* is the shear stress velocity of a uniform flow with mean velocity V.

From the differential equation (22) the difference equation (29) can be derived, in which c' denotes the concentration at time $t + \Delta t$ and c at time t:

$$\frac{c'(z_*) - c(z_*)}{\Delta t_*} = \varepsilon_*(z_*) \frac{c(z_* + \Delta z_*) - 2c(z_*) + c(z_* - \Delta z_*)}{(\Delta z_*)^2}$$

$$+ \frac{\varepsilon_*(z_* + \Delta z_*) - \varepsilon_*(z_* - \Delta z_*)}{2\Delta z_*} + w_* \frac{c(z_* + \Delta z_*) - c(z_* - \Delta z_*)}{2\Delta z_*} \qquad (29)$$

The computation of c has been carried out in the same way as the calculation of p_*, described in appendix A. First p_* is calculated in all points of the wanted grids at a certain time t_*, and after that ε_* (from (27)) and c in the same way in the same points at the same time. Values of c smaller than zero are replaced by zero. As initial condition has been taken: $p_* = c \equiv 0$; the boundary condition at z^*_{max} is $c = p \equiv 0$.

The bottom boundary condition remains a problem in its own, which will be investigated later on. In the exemple, given in fig. 6, some arbitrary function has been chosen. The concentration has been chosen equal to the probability that the lift force on a particle is larger than its own weight. For this probability p_r was found by KALKANIS[11] (using the well-known EINSTEIN-aproach[12]:

$$p_r = \frac{1}{\sqrt{2\pi}} \int_{B_*\psi - \frac{1}{\eta_*}}^{\infty} e^{-z^2} dz \qquad (30)$$

where ψ is proportional to the ratio between the lift force and the own weight:

$$\psi = \Delta \frac{gD}{u_n^2} \qquad (31)$$

where Δ is the relative specific density $(\rho_s - \rho)/\rho$, D is the grain diameter and u_n is the velocity at a distance 0.35 D from the theoretical bed. Relating u_n with the shear stress velocity p, assuming a logarithmic velocity distribution, one finds for a rough bed: $u_n = 5.24 \; p'$ (vide [12], p. 35, eq (45) to (46)); where p' is the part of the bottom friction τ', exerted on the

grains.

If τ' is a fraction μ (ripplefactor) of the total shear
stress, one finds:

$$\psi = \psi \min / p_*^2 \tag{32}$$

where

$$\psi \min = \frac{1}{(5.24)^2} \cdot \frac{\Delta}{\mu} \cdot \frac{gD}{p_b^2} \tag{33}$$

In (30) B_* has been taken 4 and $1/\eta_o$ equal to 1.5, follo-
wing KALKANIS [11].

Fig. 6 shows the concentration at various levels as a
function of time for an oscillatory flow without current. Fig.
7 shows the velocity distribution and the sediment transport,
i.e. concentration times velocity for an oscillatory flow
with resultant current.

5. Conclusion.

It may be expected, that the computer programs under
development [1] may   provide a powerful tool in the under-
standing of unstationary periodical water- and sediment motion.
Careful testing on data will be obligatory. Already a better
insight in the water motion of an oscillatory current with a
resultant flow has been obtained (ch. 3).

Appendix A.

The numerical computation according to the explicite
method.

The differential equation (11) can be written as the fol-
lowing difference equation, relating the value of p_* after one
increment of time to the original value of p_* in the same
point and in the two adjacent points.

$$p_* [z_*, t_* + \Delta t_*] = p_* [z_*, t_*] +$$

$$+ \frac{z_* (\Delta t_*)}{(\Delta z_*)^2} \quad p_* [z_* - \Delta z_*, t_*] \cdot abs (p_* [z_* - \Delta z_*, t_*])$$

$$-2 p_* [z_*, t_*] \cdot abs (p_* [z_*, t_*])$$

$$+ p_* [z_* + \Delta z_*, t_*] \cdot abs (p_* [z_* + \Delta z_*, t_*]) \tag{A1}$$

In (A1) the factor $\Delta t_* / (\Delta z_*)^2$ can be chosen arbitrary,
with the limitation, that numerical instabilities have to be
avoided. From the solution of similar linear differential
equations this appears to include the condition:

---

[1] Details about the programs are given in the internal re-
ports [8] and [13].

$$\Delta t_* \leq \frac{(\Delta z_*)^2}{2\ p_{*max} \cdot z_{max}} \tag{A2}$$

in which: p_{*max} = the maximum p_* which occurs. This maximum is
found at the bottom and equals 1.

z_{*max} = the maximum z_* for which the computation is carried out. As stated in ch. 2, z^*_{max} mostly equals 1.

As the boundary condition will be: U=0 at z=.03 times the ripple height r, near the bottom a maximum grid height Δz=.03 r/Z=.03 $r/2\pi x\ a\sqrt{f_*/2}$ will be required. For a reasonable value r/a=400 this would make Δz_* of the order 1/3 000. Then from (A2) it appears, that a maximum Δt_* is required, equal to $10^{-6}/18$. Calling a "basic calculation" the calculation of one value of p_* [z_*, t_*+ Δt_*] according to (A1), the required number of basic calculations which have to be carried out for only one wave period would be of the order 3 000x18x10^6= 54x10^9, which is very much, even for a computer.

Therefore, a more economic way of computation had to be developed, which is called: the method of the "pulsating grid".

	BOUNDARY CONDITION ↓					HEIGHT ABOVE THE BOTTOM $z_*/\Delta z_*$ →		
	1	4	8	12	16	20	24	32
t (t/Δt divisible by 8)	1 2 3 4 5	①	② ③ ④ ⑤					
		I	II III IV V					
			ⓘ		ⓘⓘ		ⓘⓘⓘ	ⓘⓥ
t +Δt	1 2 3 4							
t + 2Δt	1 2 3 4 5	① ② ③ ④						
t + 3Δt	1 2 3 4							
t + 4Δt	1 2 3 4 5	① ② ③ ④ ⑤						
		I	II III IV					

fig. A1.   Schedule of calculations according to the pulsating grid.

This system gives a high accuracy and much information near the bottom and relatively less far from the bottom.

For this aim a small grid length Δz_* has been chosen near the bottom (fig. A1), consisting of 5 points 1 to 5. When the number of time steps $n=t_*/\Delta t_*$ was odd, calculations were carried out in this grid. When the number n was divisible by 2 but not by 4 however, calculations were carried out also in a grid with a double grid length, consisting also of 5 points

①to ⑤(fig. A1). When n was divisible by 4 but not by 8, the width of the grid was doubled again (points I to V) and calculations were carried out in the smallest, the medium and the largest grid, etc.

Thus of the total number of grids equals m, the first four points of the last one cover the whole stretch from $z_* = 0$ to $z_* = 1$ and the first one has a length of $\frac{5}{4}.2^{-m+1}$. The distance Δz_* equals one fifth of the length of the smallest grid, i.e. 2^{-m-1}.

The maximum z_* of the smallest grid is $5 \times 2^{-m-1}$, and therefore, according to (A2), the maximum time step, which does not give instabilities will be:

$$\Delta t_* = 2^{-m-5} \text{ with } \Delta z_* = 2^{-m-1} \tag{A3}$$

Eq (A2) shows one of the advantages of the chosen system: because z^*_{max} is taken never more than 5 times Δz_*, Δt_* is proportional to Δz_* instead of proportional to $(\Delta z_*)^2$.

It can be easily shown[8], that when $\Delta t_* = 2^{-m-5}$, the number of basic calculations per wave period will be of the order $128/\Delta z_*$. In the case Δz_* equals 1/3 000, this number becomes 400 000, being a very small fraction of the original number of calculations. This indicates, that the more intricate way of programming is feasible.

The following schedule of computations is used (fig. A1). Assume the values of p_* in the points 1 to 5, ① to ⑤ and I to V at time t are known and that t is divisible by 8.

At time $t + \Delta t$, the points 2, 3 and 4 are found from point 1, 2, 3, 4, 5 at time t, using eq (A1). Point 1 at time $t + \Delta t$ is found from the boundary condition, point 5 is not calculated.

At time $t + 2\Delta t$ the following calculations are carried out (fig. A1). Point 2, 3 are calculated from point 1, 2, 3, 4 at time $t + \Delta t$, using eq (A1); point ②, ③, ④ are found from point ①, ②, ③, ④, ⑤ at time t, using eq (A1) with double values of Δy and Δt. Point 1 at time $t + 2\Delta t$ is found from the boundary condition at the bottom; p_* at point ① equals the calculated value in point 2 (fig. A1), point 4 equals point ②, point 5 is found by extrapolating between ② and ③, using an extrapolation formula:

$$p_5 = (-p_3 + 4\tfrac{1}{8} p_② + 3\tfrac{1}{4} p_③ - \tfrac{3}{8} p_④)/6 \tag{A4}$$

(A4) relates the values of p_* in the smaller and the larger grids; all values apply for the same time. The index indicates the grid point. In (A4) the indices surrounded by a circle denote the values in a larger grid, the indices without a circle in a smaller grid.

Now the way of calculation will be clear: at time $t + 3\Delta t$ only calculations in the smallest grid are carried out; at time $t + 4\Delta t$ the same schedule of $t + 2\Delta t$ is followed, only up to one grid larger: the points II, III, IV are found from I, II, III, IV, V at time t, the points ②, ③ from point ①, ②, ③, ④ at time $t + 2\Delta t$, the points 2, 3 from point 1, 2, 3, 4 at time $t + 3\Delta t$. Point ④ equals point II, point ⑤ is interpolated between II and III. Point 4 equals point ②, point 5 is interpolated between ② and ③. Point ① equals point 2, point I equals point ②, point 1 is found from the boundary condition.
Now the following time step can be calculated, etc.

Literature.

[1] Vanoni V.A.
    Transportation of suspended sediment by water. Trans.
    Amer. Soc. Civ. Engrs. 111 p. 67-133   (1946)
[2] Prandtl, L.
    Abrisz der Stromungslehre, Braunschweig, 3er Abschnitt (1931)
[3] Karman, Th. von
    Mechanische Ahnlichkeit und Turbulenz. Proc. 3rd Int.
    Congress for Appl. Mech. Vol I p. 85-92   (1930)
[4] Jonsson, I.G.
    On the existence of universal velocity distributions in
    an oscillatory, turbulent boundary layer. Techn. Univ. of
    Denmark, Basic Res. Progress report no. 12   (1966)
[5] Radder, K.W. and Geilvoet, W.
    Snelheidsverdeling in een oscillerende stroom (velocity
    distribution in an oscillatory flow). Techn. Univ. of
    Delft, M. Sc. Thesis (unpublished)   (1973)
[6] Jonsson, I.G.
    Measurements in the turbulent wave boundary layer. 10th
    I.A.H.R. Congress, London I, p. 85-92   (1963)
[7] Jonsson, I.G.
    Wave boundary layers and friction factors. Proc. 10th
    Conf. Coastal Engng, Tokyo p. 127-149   (1967)
[8] Bakker, W.T.
    Bottom friction and velocity distribution in an oscilla-
    tory flow. Rijkswaterstaat, Dir. for Hydr. Res. and Water
    Management, Dept. for Coastal Res., Memo 72-23^{b} (internal
    report)   (1972)
[9] Proudman.
    Dynamical Oceanography (§ 151)   (1953)
[10] Jonsson, I.G. and H. Lundgren,
    Derivation of formulae for phenomena in the turbulent wave
    boundary layer. Techn. Univ. of Denmark, Basic Res. Pro-
    gress report no. 9   (1965)
[11] Kalkanis, G.
    Transportation of bed material due to wave action. Coast.
    Engng. Res. Center, Techn. Memo. no. 2.   (1964)
[12] Einstein, H.A.
    The bed-load function for sediment transportation in open
    channel flow. U.S. Dept. of Agr.; Techn. Bull. no. 1026 (1950)
[13] Bakker, W.T.
    Sand concentration in an oscillatory flow. Rijkswater-
    staat, Dir. for Hydr. Res. and Water Management , Dept.
    for Coastal Res., Memo 72-28^{a} (int. rep.)   (1973)
[14] Kajiura, K.
    A model of the bottom boundary layer in water waves. Bull.
    Earthg. Res. Inst. 46, (pp) 75-123   (1968)
[15] Manohar, M.
    Mechanics of bottom sediment movement due to wave action.
    Beach Erosion Board, Techn. Mem. 75   (1955)